Shape evolution with temperature of a thermotolerant protein (PeaT 1) in solution detected by small angle X-ray scattering

ARTICLE *in* PROTEINS STRUCTURE FUNCTION AND BIOINFORMATICS · JANUARY 2013

Impact Factor: 2.63 · DOI: 10.1002/prot.24162 · Source: PubMed

13 AUTHORS, INCLUDING:

Xueqing Xing
Chinese Academy of Sciences
28 PUBLICATIONS **137** CITATIONS
SEE PROFILE

Wei Wang
Beijing Medical University
121 PUBLICATIONS **1,038** CITATIONS
SEE PROFILE

Weidong Cheng
Chinese Academy of Sciences
11 PUBLICATIONS **34** CITATIONS
SEE PROFILE

Zhonghua Wu
Chinese Academy of Sciences
211 PUBLICATIONS **1,437** CITATIONS
SEE PROFILE

PROTEINS
STRUCTURE ■ FUNCTION ■ BIOINFORMATICS

Shape evolution with temperature of a thermotolerant protein (*PeaT*1) in solution detected by small angle X-ray scattering

Xueqing Xing,[1,2] Quan Liu,[3,4] Wei Wang,[1] Kunhao Zhang,[1] Tang Li,[3] Quan Cai,[1] Guang Mo,[1] Weidong Cheng,[1,2] Dehong Wang,[1,2] Yu Gong,[1,2] Zhongjun Chen,[1] Dewen Qiu,[3]* and Zhonghua Wu[1,2]*

[1] Beijing Synchrotron Radiation Facility, Institute of High Energy Physics, Chinese Academy of Sciences, Beijing 100049, People's Republic of China

[2] Graduate University of Chinese Academy of Sciences, Beijing 100049, People's Republic of China

[3] State Key Laboratory for Biology of Plant Diseases and Insect Pests, Institute of Plant Protection, Chinese Academy of Agricultural Sciences, Beijing 100081, People's Republic of China

[4] College of Life Science and Technology, Heilongjiang Bayi Agricultural University, Daqing 163319, People's Republic of China

ABSTRACT

The protein elicitor from *Alternaria tenuissima* (*PeaT*1) presented excellent thermotolerance and potential application in agriculture as a pesticide. Previous synchrotron radiation circular dichroism study demonstrated that the secondary structures in *PeaT*1 protein are reversible with temperature change. To further clarify the mechanism of its thermotolerance, synchrotron radiation small angle x-ray scattering (SAXS) technique was used to study the shape change of *PeaT*1 protein with temperature in this article. *Ab initio* structure restorations based on the SAXS data revealed that *PeaT*1 protein has a prolate shape with a P_2 symmetry axis along the prolate anisometric direction. With temperature increase, a gooseneck vase-like (25°C), to jug-like (55°C), then to oval (85°C) shape change can be found, and these shape changes are also approximately reversible with temperature decrease. *PeaT*1 protein contains two homogenous molecules, and each of them consists of *F*, *NAC*, *T*, and *UBA* domains. The structures of the four domains were predicted. Simulated annealing algorithm was used to superimpose the domain structures onto the SAXS shapes. It was found that all the structural domains have position rotation and translation with temperature change, but the *NAC* domains are relatively stable, playing a role of frame. This shape change information provides clues for further exploring its biological function and application.

Proteins 2013; 81:53–62.

Key words: domain; structure restoration; structure prediction; SRCD; SAXS; *PeaT*1.

INTRODUCTION

Alternaria tenuissima is a saprophytic fungal pathogen, which is often used as an etiological agent among various plant diseases.[1] In a previous research, Protein Elicitor from *A. tenuissima* (*PeaT*1) cloned at the State Key Laboratory for Biology of Plant Diseases and Insect Pests of China from *A. tenuissima* (GenBank accession No. EF030819) was found enhancing the tolerance of tobacco against TMV (tobacco mosaic virus).[2] Especially, when *PeaT*1 protein solution was heated in boiling water bath, it was unexpected that there was no deposition appearing, and the capability of *PeaT*1 to enhance the tolerance of tobacco against TMV was still kept after heating. Obviously, such a thermotolerance can provide great convenience for *PeaT*1 application as a biological

Abbreviations: BSRF, Beijing synchrotron radiation facility; SAXS, small angle X-ray scattering; SRCD, synchrotron radiation circular dichroism. Chinese Academy of Sciences.

Grant sponsor: National Natural Scientific Foundation of China; Grant number: 10385008; Grant sponsor: the Knowledge Innovation Program of Chinese Academy of Sciences; Grant number: kjcx3.syw.n8; Grant sponsor: the Momentous Equipment Program of Chinese Academy of Sciences; Grant number: YZ200829; Grant sponsor: 973 projects; Grant number: 2003CB114204; Grant sponsor: 863 projects; Grant number: 2006AA10A210; Grant sponsor: the Ministry of Science and Beijing grand project; Grant number: D706005040431; Grant sponsor: National Natural Scientific Foundation of China; Grant number: 31101485
Xueqing Xing and Quan Liu contributed equally to this work.
*Correspondence to: Zhonghua Wu, 19B Yuquan Road, Shijingshan District, Beijing 100049, Republic of China. E-mail: wuzh@ihep.ac.cn or Dewen Qiu, State Key Laboratory for Biology of Plant Diseases and Insect Pests, Institute of Plant Protection, Chinese Academy of Agricultural Sciences, Beijing 100081, People's Republic of China. E-mail: dewenqiu@hotmail.com.
Received 30 January 2012; Revised 19 July 2012; Accepted 28 July 2012
Published online 14 August 2012 in Wiley Online Library (wileyonlinelibrary.com).
DOI: 10.1002/prot.24162

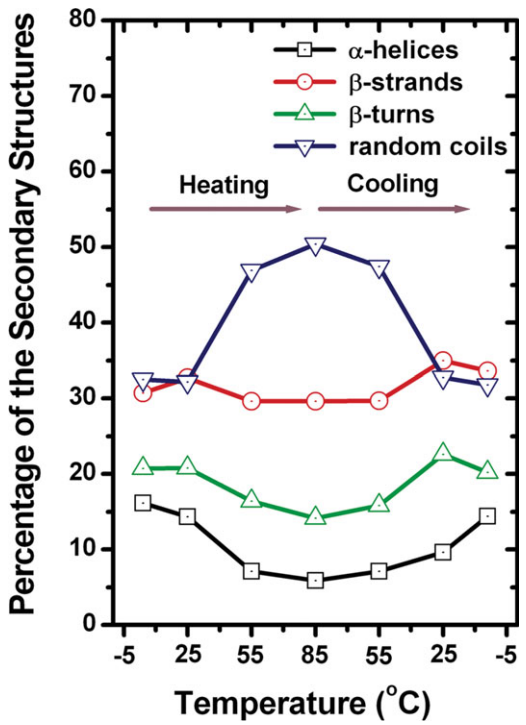

Figure 1

SRCD result: percentage changes of the secondary structures of *PeaT*1 protein in a heating–cooling cycle cited from Ref. [6]. [Color figure can be viewed in the online issue, which is available at wileyonlinelibrary.com.]

pesticide. In this study, *PeaT*1 protein is found to include four structural domains marked, respectively, as *F*, *NAC*, *T*, and *UBA* according to Pfam.[3] The amino acid sequences of the four domains are, respectively, 1–51, 52–109, 110–168, and 169–207. Among the four structural domains, the crystal structures of *NAC* and *UBA* are available. Those crystal structures can be obtained from the *aeNAC* (PDB ID: 1TR8) protein.[4,5] *NAC* domain was reported to consist of β-strands. Two *NAC* domains were found to form a β-strand barrel in the *aeNAC* homodimer. *UBA* was found to be composed of three α-helix bundles. However, the crystal structures of *F* and *T* domains are still unknown. Synchrotron radiation circular dichroism (SRCD) study[6] demonstrated that the content of β-strands in *PeaT*1 was almost a constant during the heating–cooling cycle, but the other secondary structures presented reversible changes with temperature. For convenience, the SRCD result on *PeaT*1 protein is trivially summarized in Figure 1.

Although the secondary structures of the thermotolerant *PeaT*1 protein were identified as being reversible during a heating–cooling cycle, the shape evolution with temperature of the whole protein is still unknown. The changes in relative position of the four structural domains, the possible aggregation number of *PeaT*1 molecules, as well as the ubiety of multiple molecules are also unknown. However, the shape and configuration of the four structural domains in the *PeaT*1 proteins are important and helpful to understand the thermotolerance of *PeaT*1 protein. Small Angle X-ray Scattering (SAXS) is a powerful tool to investigate the structure of biological macromolecules[7–11] in solution, especially suitable for variable environmental processes[12–14] and complex studies.[15–17] With the great improvement of the *ab initio* methods for restoring the three-dimensional shape of a macromolecule from one dimensional SAXS profile, the SAXS technique can provide a best fit model that represents the probable overall, time-averaged ensemble shape of a protein in solution under nearly physiological conditions.[18–20]

In this article, the structure of *PeaT*1 protein in solution and its shape changes with temperature are investigated with SAXS technique. On the basis of the *ab initio* approaches,[21,22] the resultant configurations of dummy atoms and the envelope shapes of *PeaT*1 protein at different temperatures are used to clarify the mechanism of the thermotolerance of *PeaT*1, which also gives the clues to further insight into its biological functions and agricultural application.

MATERIALS AND METHODS

Protein *PeaT*1 preparation

A construction for *PeaT*1 with *C*-terminally His_6-tagged was generated from cDNA using the primers 5′-CATGCCATGGGCCATCATCATCATCATCACATGGCC AACCCCCGCATT-3′ (forward) and 5′-CCGCTCGAGC TATATGCTCAGCGC CAT-3′ (reverse). The amplified PCR product was ligated into pMD18-T Vector (TaKaRa) and subcloned as an Nco1-Xho1 fragment into the Nco1-Xho1 site of pET28a (Novagen). Recombinant His-*PeaT*1 was expressed in Escherichia coli BL21 (DE3) strain. Cells were grown in LB Broth medium containing 50 mg/mL kanamycin at 310 K to an OD600 of 0.8, induced with 0.5 m*M* isopropyl-β-D-thiogalactopyranoside and grown for 6h at room temperature. The cells were then harvested and stored at 253 K until further use. The lysis was performed in the binding buffer (500 m*M* NaCl, 5 m*M* NaH_2PO_4, and 15 m*M* Na_2HPO_4, pH 7.4) by using sonication on ice. The lysate was cleared by centrifugation at 18,000 rpm for 40 min. The supernatant solution was used as the crude extract for expression and loaded onto a His-trap HP column (GE Healthcare) for affinity purification using His tag attached to the protein. 10% elution buffer (binding buffer added 500 m*M* imidazole) was used to clean nonspecific binding proteins and 40% elution buffer was used to elute the His-*PeaT*1 protein. After desalting by ultrafiltrate tube (Millipore), the protein was dissolved into the low salt buffer (20 m*M* Tris, 50 m*M* NaCl, pH 7.4). Afterwards, this protein was purified by Mono Q column (GE

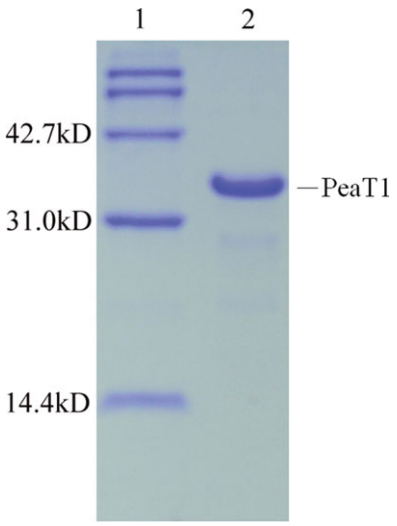

Figure 2

SDS-PAGE result of the purified *PeaT*1 protein. Lane 1: Protein molecular weight marker. Lane 2: Purified *PeaT*1. [Color figure can be viewed in the online issue, which is available at wileyonlinelibrary.com.]

Healthcare) using a linear gradient of NaCl concentration from 50 to 500 m*M*. The high purity of collections were pooled and concentrated to about 10 mg/mL. The last purification was carried out by using Superdex-200 (16/60) size-exclusion column chromatography (GE Healthcare). Then the purified His_6-tagged *PeaT*1 protein was concentrated to 30.00 mg/mL, 7.50 mg/mL and 3.75 mg/mL for further use. These protein concentrations were determined by measuring the UV absorptance with wavelength of 280 nm.[23] A molar extinction coefficient of 6990 M^{-1} cm^{-1} was used in the calculation. The purity of His_6-tagged *PeaT*1 protein is confirmed to be higher than 90% by the SDS-PAGE gel as shown in Figure 2. The apparent molecular weight of *PeaT*1 on SDS-PAGE is estimated to be about 35 kDa.

SAXS measurements

During the heating–cooling cycle, *in-situ* SAXS data of *PeaT*1 protein in 50 m*M* Tris buffer (pH 8.0) containing 50 m*M* NaCl were collected at beamline 1W2A of the Beijing synchrotron radiation facility (BSRF) with the protein concentrations of 3.75, 7.50, and 30.00 mg/mL. Two-dimensional CCD detector was utilized to record the SAXS intensities. *PeaT*1 protein solutions were injected into a well-prepared sample cell with two parallel x-ray windows of laminated mica. The thickness of sample cell is 1 mm and the sample volume is about 70 μL. Such a sample cell was connected to a water heating–cooling system to control the sample temperature. The SAXS patterns of the pure buffers and *PeaT*1 protein solutions were alternately collected in an exposure time of 150–600s to avoid radiation-induced protein damage. The sample-to-detector distance was fixed at 1500 mm, covering a scattering vector (q) range of 0.1–2.1 nm^{-1}. Where $q = 4\pi\sin\theta/\lambda$, 2θ is the scattering angle; λ is the x-ray wavelength (1.54Å) monochromatized by a triangle bending Si (111) monochromator. *PeaT*1 protein solutions were heated to 25, 55, 85, 55, and 25°C in sequence. The corresponding SAXS patterns were collected at the above five temperatures, respectively. The samples were thermally stabilized for about 5 min before every SAXS measurement. The SAXS patterns were measured at least thrice at each temperature to control radiation damage and protein thermal stability. The sample environments in SAXS measurements are almost the same as in previous SRCD measurements.

RESULTS AND DISCUSSION

SAXS data

SAXS data pretreatment

The SAXS patterns were firstly transformed to one-dimensional SAXS curves by using the Fit2d program.[24] After normalizing the SAXS intensities to the direct beam intensities and removing the buffer scattering from the solution scattering, the SAXS scattering intensities from *PeaT*1 protein were respectively isolated. Then, these SAXS intensities were normalized to a constant concentration of 1 mg/mL. It was found that the low concentration (3.75 mg/mL) SAXS curves have the same profiles with the higher concentration (7.50 mg/mL) SAXS curves except slightly larger noise. The SAXS data and the Guinier plots of the samples at room temperature with concentrations of 3.75 and 7.50 mg/mL are compared in Figure 3. The similar SAXS profiles and almost the same linear behaviors in Guinier region means that the interaction or interference effect between protein particles is neglectable as the concentration is lowered from 30 mg/mL to 7.50 mg/mL. Therefore, the SAXS data with concentration of 7.50 mg/mL were used for further data analysis. Except different noise levels, the SAXS profile at high-q end is hardly affected by the alteration of protein concentration. To depress the unwanted data noise, three independent SAXS measurements at least were averaged at each temperature. At the same time, the high-q SAXS data with concentration of 30 mg/mL were merged into the SAXS data with concentration of 7.50 mg/mL by using PRIMUS.[25] Finally, the resultant SAXS curves at the measurement temperatures (25, 55, 85, 55, and 25°C) were obtained and marked as 251, 551, 851, 552, and 252, respectively, as shown in the left panel (hollow squares) of Figure 4.

Scattering data analysis

Gyration radius R_g and zero angle intensity $I(0)$ are two important parameters that can be extracted from the SAXS data. R_g is related to the size of protein particle in

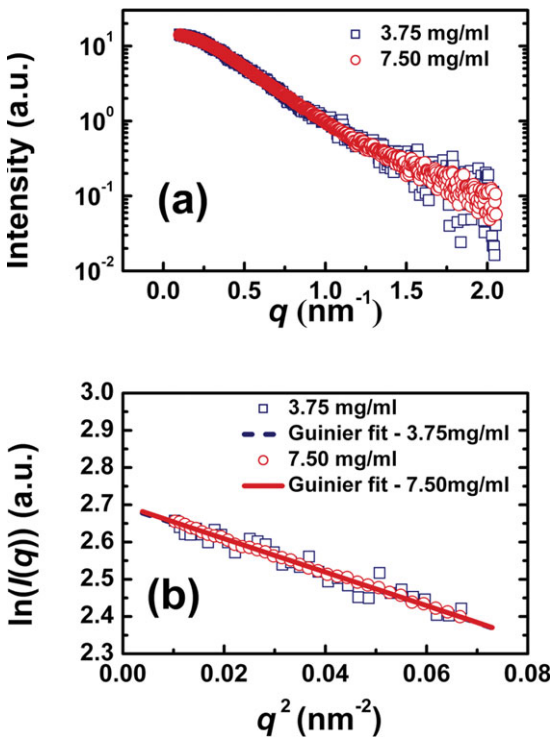

Figure 3

Concentration-normalized SAXS intensities (**a**) and Guinier plots (**b**) of 3.75 mg/mL (Open squares) and 7.50 mg/mL (Open circles) at 25°C. [Color figure can be viewed in the online issue, which is available at wileyonlinelibrary.com.]

solution. $I(0)$ is in direct proportion to the product of protein concentration c and particle mass M for a monodisperse and dilute solution[26] as shown in Eq. (1).

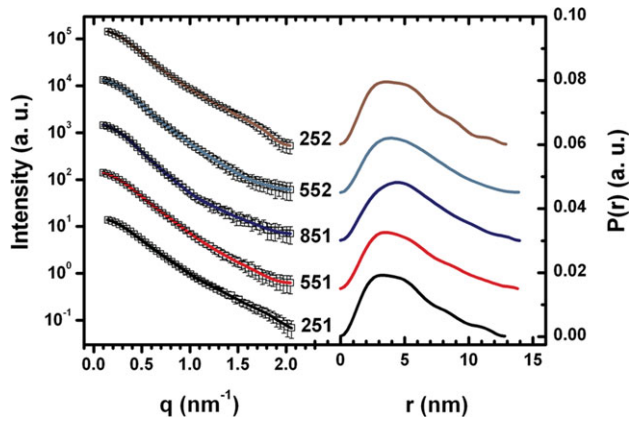

Figure 4

SAXS and P(r) profiles: Left: Experimental SAXS intensities (symbols) and their DAMMIN fitting curves (solid lines); Right: Distance distribution function $P(r)$. Numerals 251, 551, 851, 552, and 252 mark, respectively, the protein being heated to 25, 55, and 85°C, then cooled to 55 and 25°C. [Color figure can be viewed in the online issue, which is available at wileyonlinelibrary.com.]

$$I(0) = \frac{cN_AM}{\mu^2}(1 - \rho_0\psi)^2. \quad (1)$$

where N_A is Avogadro's number, μ is the ratio of the molecular weight to the number of electrons of the particle, ρ_0 is the average electron density of the solvent, and ψ is the ratio of the volume of the particle to its number of the electron. The parameters R_g and $I(0)$ can be easily obtained from the slope and intercept of the Guinier plot ($\ln I(q) \propto q^2$ at low-q end).[27] However, more accurate values of R_g and $I(0)$[26] can be evaluated from the $P(r)$ function. In contrast with the momentum-space SAXS curve $I(q)$, the real-space function $P(r)$ is easier to be understood, which is a measure of the frequency of inter-atomic vector lengths within a particle. $P(r)$ contains the same structure information as the momentum-space SAXS curve $I(q)$. Usually, $P(r)$ function can be described as the Fourier transform of the SAXS curve $I(q)$[27] as shown in Eq. (2).

$$P(r) = \frac{1}{2\pi^2}\int_0^\infty I(q)\cdot(qr)\cdot\sin(qr)\cdot dq. \quad (2)$$

The $P(r)$ functions of *PeaT*1 protein in the solutions with different temperatures were calculated by using the indirect Fourier transform program GNOM[28–30] in a q-range of 0.–1–2.1 nm^{-1} as shown in the right panel of Figure 4. Based on these $P(r)$ functions, the average values of R_g, $I(0)/c$ and the maximum dimension (D_{max}) of the scattering particles were obtained for *PeaT*1 protein with different temperatures as listed in Table I. To estimate the particle mass of *PeaT*1 protein in the solution, the SAXS pattern of a *BSA* (bovine serum albumin) solution with concentration of 10 mg/mL was also measured in the same experimental condition. The particle mass of *BSA* is known to be 67 kDa.[31] By comparing the concentration-normalized $I(0)/c$ between *BSA* and *PeaT*1, the particle mass of *PeaT*1 protein at 25°C is about 47 kDa.

Table I

R_g and $I(0)/c$: Radius of Gyration and Maximum Dimension of *PeaT*1 Protein Homodimer as Well as Concentration-Normalized Scattering Intensity at Zero Angle $I(0)/c$ Calculated From the Distance Distribution Functions $P(r)$ by GNOM at the Measurement Temperatures

Protein	Temperature	R_g (Å) From P(r) function	D_{max} (Å) Maximum dimension	$I(0)/c$ From P(r) function
*PeaT*1	Initial at 25°C	39.9 ± 1.2	128.0 ± 2.0	15.69 ± 0.45
	Heated to 55°C	42.0 ± 2.3	138.0 ± 2.0	14.69 ± 0.89
	Heated to 85°C	44.0 ± 1.9	139.0 ± 3.0	15.71 ± 0.63
	Cooled to 55°C	42.0 ± 0.2	139.0 ± 3.0	14.34 ± 0.50
	Cooled to 25°C	40.4 ± 0.7	129.0 ± 2.5	16.48 ± 0.29
BSA	25°C			22.30 ± 0.88

R_g is the radius of gyration; D_{max} is the maximum dimension; $I(0)$ is the scattering intensity at zero angle; c is the concentration of *PeaT*1 protein.

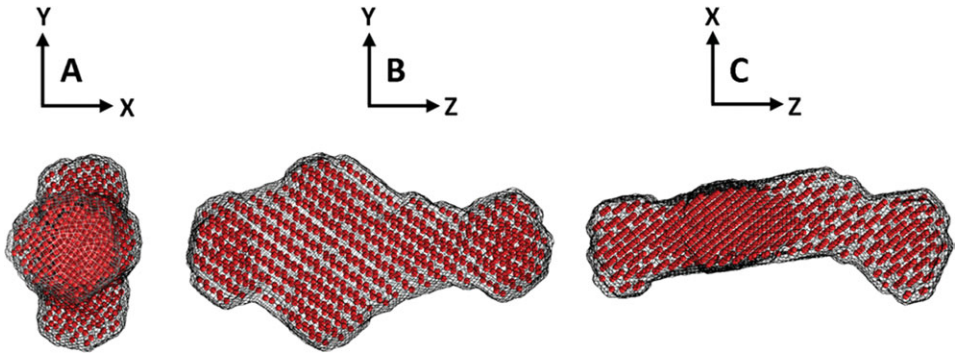

Figure 5

*PeaT*1 shape: Average *PeaT*1 protein shape (at 25°C) of 12 configurations in DAMMIN calculations without any constraint, which implies that an approximate P_2 symmetrical axis is along the anisometric direction of the prolate shape of *PeaT*1 protein [Color figure can be viewed in the online issue, which is available at wileyonlinelibrary.com.].

While the calculated mass of one *PeaT*1 molecule from the amino acid sequence is about 23.5 kDa, including the six His-tags. It demonstrates that the particle mass of *PeaT*1 protein is about twice its molecule mass. Therefore, it can be concluded that *PeaT*1 protein exists as a homodimer in the solution. From Table I, the particle mass of *PeaT*1 was estimated to distribute in a range from 43 to 49 kDa for the samples at other temperatures. The average mass of *PeaT*1 proteins in the solution with various temperatures is about 46 kDa. The mass fluctuation of the *PeaT*1 protein particles is about 6% with temperature change. This fluctuation can be ascribed to the change of particle shape (or volume) and the solvent density with temperature according to Eq. (1). All these demonstrate again that *PeaT*1 particles in the solution are always in homodimeric form, which excludes the concentration-dependent aggregation at all the measurement temperatures. The homodimeric attribute of *PeaT*1 protein in the solution validates the monodispersity of the samples. Although the SDS-PAGE gel confirms the purity of *PeaT*1 protein is higher than 90% as shown in Figure 2, the apparent molecular weight (35 kDa) of *PeaT*1 on SDS-PAGE is obviously larger than the calculated value (23.5 kDa) from the known amino acid sequence. This difference between the calculated molecular mass and the apparent one can be attributed to an unusual running behavior in SDS-PAGE. A similar unusual running behavior[31] was also reported for the *NAC* proteins. Where two kinds of *NAC* proteins shown the molecular weights[31,32] of 33 kDa and 22 kDa on SDS-PAGE, but their calculated values were 23.492 kDa and 17.352 kDa, respectively.

Besides, *PeaT*1 homodimers in the solution can be approximately thought to take prolate shapes at the measured temperatures. This is because an elongated particle has a skewed distribution[14,33] in its $P(r)$, and a clear maximum at smaller distance, corresponding to the radius of the cross-section as shown in the right panel of Figure 4.

Shape reconstructions

The overall shapes of *PeaT*1 homodimer in the solution can be restored through their $P(r)$ functions by using the well-established reconstruction method DAMMIN.[34] The starting model is a sphere with diameter being equal to the maximum particle size. This sphere is filled by about $M\sim1000$ densely packed small beads (dummy atoms). These dummy atoms form a configuration vector **X** (binary vector, 1 means that the dummy atom belongs to the particle, and 0 to the solvent, length M). By minimizing the discrepancy function $f(X) = \chi^2 + \alpha P(X)$, DAMMIN can search for the best configuration of the dummy atoms. Where, $P(X)$ is a looseness penalty to ensure the compactness and connectivity of the solution with a positive weight α. χ is the discrepancy between the experimental scattering intensity I_{exp} and the calculated curve I_{cal} as defined in Eq. (3).

$$\chi^2 = \frac{1}{N-1}\sum_j \left[\frac{I_{\exp}(q_j) - cI_{cal}(q_j)}{\sigma(q_j)}\right]^2. \qquad (3)$$

where N is the number of experimental points, c is the scaling factor, and $\sigma(q_j)$ is the experimental error at the scattering vector q_j. During the SAXS curve fitting, the coordinates of beads are randomly modified to approach the optimal configurations and decrease the discrepancy $f(X)$.

To estimate the shape of *PeaT*1 homodimers in the solution, we did DAMMIN calculation with none constraint at first. Twelve configurations from independent DAMMIN runs were averaged for *PeaT*1 protein at the initial 25°C. The average configuration took a prolate shape and had an approximately two-fold symmetrical axis along the prolate anisometric direction as shown in Figure 5. This implies that a P_2 symmetry exists in *PeaT*1 protein shape. Therefore, it is reasonable to assume a P_2 symmetry constraint in DAMMIN calculation. Based on

the above SAXS data analysis, a P_2 symmetry and the prolate anisometry were used in the following *ab initio* reconstructions. In addition, the anisometric axis of the shape was also, respectively, constrained to be parallel (along) or perpendicular to (across) the P_2 axis. It was found that when the anisometric axis was constrained to be along the P_2 axis, the obtained configurations are always similar, but when the anisometric axis was constrained to be across the P_2 axis, the resultant configurations are nonexclusive and nonconvergent. This means that taking the anisometric axis as the P_2 symmetrical axis is stable and reasonable. In addition, it is also frequent that a homodimer has a P_2 symmetrical axis. Therefore, the anisometric axis was chosen as the P_2 axis in the shape reconstructions of *PeaT*1 protein.

To increase the statistic of the shape reconstruction, 12 independent DAMMIN configurations were, respectively, collected for *PeaT*1 protein at each temperature. The 12 independent configurations were aligned and averaged by using the programs SUPCOMB[35] and DAMAVER.[36] These two programs can superimpose the 12 independent configurations and filter out an average configuration, yielding the most probable particle model. The calculated SAXS intensity curves $I(q)_{cal}$ for the average configurations at different temperatures are all excellently in agreement with their respective experimental intensities as shown in the left panel (solid lines) of Figure 4. The final envelope shapes of *PeaT*1 protein were obtained from the average configurations, which can be visualized with a 3D molecular graphical program RASMOL[37] as shown in Figure 6. It is interesting that a concave appears approximately on the same location of the average configurations at all the measurement temperatures.

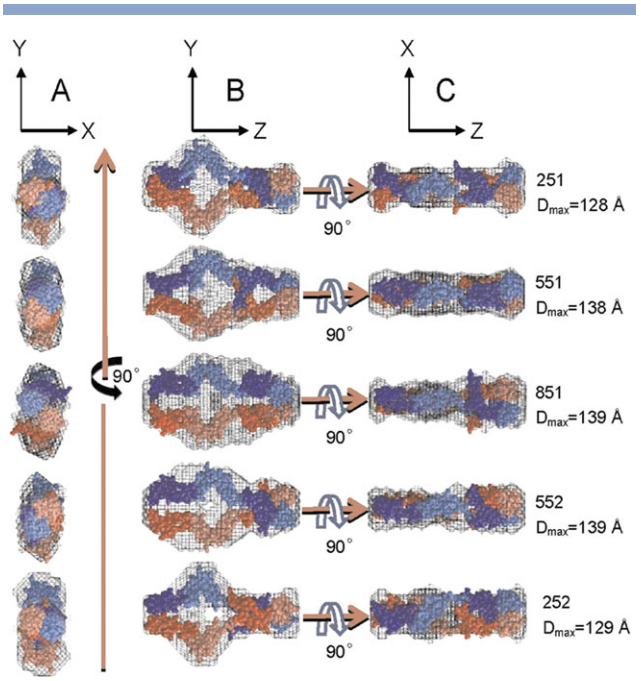

Figure 6

Shape evolution of *PeaT*1 protein with temperature and the superimposition of the domain structures with the shapes. *Z*-axis is along the prolate anisometric direction of the shapes. *X*-axis is normal to *Z*-axis and defined as the shortest direction of the shapes, *Y*-axis is orthogonal to the *X*-axis and the *Z*-axis. The top view, side view, and front view of *PeaT*1 protein shapes are, respectively, shown in column A, B, and C as mesh maps. *PeaT*1 protein was, respectively, heated to 25, 55, and 85°C, and then was cooled to 55 and 25°C, being marked as 251, 551, 851, 552, and 252. The "crystal" structures of two *PeaT*1 homogenous molecules are distinguished by the warm and cool colors and are displayed in "spacefill" mode of the RASMOL. Each *PeaT*1 molecule includes *F*, *NAC T* and *UBA* four structural domains shown in different color shades. The domain positions in *PeaT*1 protein were optimized with the simulated annealing algorithm.

Shape verification

To verify *PeaT*1 shapes reconstructed from the SAXS data in the DAMMIN calculation, the superimposition of the four structural domains (*F*, *NAC*, *T*, and *UBA*) on the overall shapes of *PeaT*1 is necessary. Because of the high homology of the *NAC* and *UBA* domains between *PeaT*1 and *aeNAC* proteins, the known crystal structures of *NAC* and *UBA* domains in *aeNAC* protein can be directly used for the shape analysis. However, the crystal structures of domains *F* and *T* are still unknown. Fortunately, the homology modeling-based tertiary structure prediction[38] can be used to predict the crystal structure of domain *T*. Unfortunately, domain *F* consists mainly of the secondary structures of random coils. There is no homology model suitable for the domain *F* up to now. In this case, a predicted ordinate structure of domain *F* can just be obtained from the amino acid sequence.[38] To check the reliability of the predicted structures, the possible structures of domains *NAC* and *UBA* were firstly predicted and testified to be almost the same as in *aeNAC* protein. The predicted structures of the four domains and their changes with temperature will be further discussed later.

To compare the shape of *PeaT*1 protein obtained from SAXS with the two *PeaT*1 molecule structures (each molecule contains *F*, *NAC*, *T*, and *UBA* four structural domains), a simulated annealing algorithm routine (OVERLAP) was used to overlap the SAXS shape with the domain structures. A detailed description about the "OVERLAP" routine will be published elsewhere. In this shape verification, total eight structural domains distributed in two *PeaT*1 molecules are needed because of the homodimeric attribute of *PeaT*1 protein in the solution. As using the routine to overlap the SAXS shape with the molecular structures, two *PeaT*1 molecules were constrained to have a P_2 symmetrical axis along the prolate anisometric direction. The eight structural domains were allowed to rotate and translate, respectively. The four structural domains were constrained to contact together according to the amino acid sequence. A penalty factor

was used to ensure the domains neither over-compact nor over-loose. An overlap between SAXS shape and the domain structures for *PeaT*1 protein at the initial 25°C is shown in Figure 6 and marked as 251. It can be seen that the SAXS shape is well in agreement with the domain structures. The concave on the SAXS envelope shape is located at the position of the two *NAC* domains from the two molecules of *PeaT*1 homodimer. The two *NAC* domains hug together, leaving a concave between them. This tells clearly us that the two *NAC* domains in *PeaT*1 homodimer formed a similar structure of the flattened β barrel as in *aeNAC* protein.[5] It is such a structure that results probably in *PeaT*1 protein having a quite good thermotolerance.[6] The calculated gyration radii from the SAXS shape and from the domain structures are almost the same. By this shape overlap, *PeaT*1 protein shape in the solution is verified to be reasonable and reliable.

Shape evolution

The overall shape of *PeaT*1 protein changes with temperature are shown in Figure 6. From the initial 25°C to the highest temperature 85°C, then to the final room temperature 25°C, the shape change of *PeaT*1 protein in the solution experiences an approximately reversible process. Three directional views of *PeaT*1 protein are, respectively, compared in the column A, B, and C of Figure 6. For convenience, the longest direction of the prolate shape (i.e., the P_2 symmetry axis) is defined as the Z axis, while the shortest direction is defined as the X axis, another orthogonal direction is defined as the Y axis. From Figure 6, it can be seen that *PeaT*1 protein has approximately a flattened shape in the Y-Z plane. The shape change occurs mainly in the Y-direction. By comparing the shape change in the Y-direction, we found that the shape of *PeaT*1 protein changed from an initial gooseneck vase-like shape (25°C) to a jug-like shape (55°C), then to an oval shape (85°C) with the temperature increase. When *PeaT*1 protein solution was cooled to 55°C and 25°C in turn, the protein shape was recovered from the oval shape (85°C) to the jug-like shape (55°C), then to the gooseneck vase-like shape (25°C). Although the *PeaT*1 protein shape experienced an approximate reversible change with temperature and this reversible change is very similar with the changes of the secondary structures obtained from SRCD, it does not predicate that the structural change of *PeaT*1 protein is also reversible at the molecular level. Because of the lack of specificity or resolution of SAXS and SRCD techniques, both techniques fall short of giving complete details of the structural changes of *PeaT*1 proteins at the molecular level. However, the information of shape evolution with temperature is still helpful to understand the thermotolerance of *PeaT*1 protein.

*PeaT*1 homodimers have a prolate shape with the prolate anisometric axis along their respective long axis. The other two orthogonal axes have also different dimensions. In fact, a concave left on the Y-Z surface of the protein shape always locates at the site of the two *NAC* domains hugged together face to face, which means that the two *NAC* domains form a stable structure. It is known that *NAC* domain contains mainly β-strands, the structural stability of *NAC* domains in *PeaT*1 protein demonstrates that the interaction between β-strands is stronger than the other secondary structures. SRCD results also demonstrated that the percentage composition of β-strands is less changed with temperature. Therefore, we believe that the stronger interaction between two *NAC* domains composed of β-strands is the origin of the thermotolerance of *PeaT*1 protein. If the two *NAC* domains are completely detached or their structures are completely destroyed, *PeaT*1 protein will degenerate to lose completely its thermotolerance. Although the hugged structure of two *NAC* domains is relatively stable in *PeaT*1 protein, a slight shift and rotation of the two domains with temperature is still observed from the position change of the concave. It is demonstrated that the relevant position of the two *NAC* domains in *PeaT*1 protein is slightly changeable. In addition, with the temperature increase, *PeaT*1 protein has a suitable expansion in the Y-direction, which results in the increase of the gyration radius and the protein shape change. The maximum dimensions D_{max} of *PeaT*1 protein and their errors were also estimated and listed in Table I. Although the maximum dimension D_{max} is hardly changed for the high temperature samples, the difference of D_{max} values between the room temperature and high temperature samples is still observable as considering the errors. D_{max} is increased from 128 Å at the initial status to 139 Å at the high-temperature.

To give more information about the structural change with temperature, all the SAXS shapes are needed to be overlapped, respectively, with the eight structural domains distributed in two *PeaT*1 molecules. According to the SRCD results, we can imagine that the structures of the four domains are changeable with temperature at the molecular level. In particular, the *F* domain may contribute to a more disordered structure at higher temperatures since it consists of random coils. Kratky plots of the scattered intensity can be used to reveal partially unfolded states at high temperatures. The Kratky plots of *PeaT*1 protein at 25–85°C are shown in Figure 7. It can be seen that these Kratky plots are not the bell-shaped curves, which means that *PeaT*1 protein is not in perfect folded states and are not globular particles at all the temperatures. And the unfolded parts in *PeaT*1 particles increase slightly with the temperature increasing. This implies again that the domain structures are changeable with temperature at the molecular level. Unfortunately, there are no available crystal structures of the four domains at various temperatures up to now. In this case, we have to use the predicted structures of the four

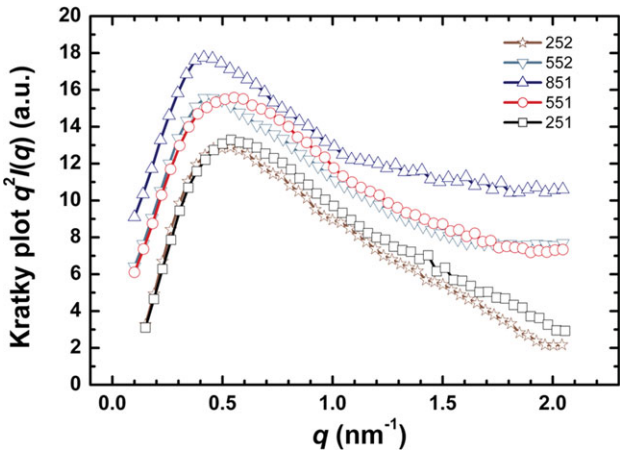

Figure 7

Kratky plots of *PeaT*1 proteins at 25, 55, and 85°C. Numerals 251, 551, 851, 552, and 252 mark, respectively, the protein being heated to 25, 55, and 85°C, then cooled to 55 and 25°C. [Color figure can be viewed in the online issue, which is available at wileyonlinelibrary.com.]

domains (*F*, *NAC*, *T*, and *UBA*) to overlap with the SAXS shapes at all the measurement temperatures. This means that the four domains were presumed to maintain their respective rigid bodies, only the relative positions between the domains are allowable to change with temperature during the overlap procedure. Evidently, this modeling can not reflect the structural changes of *PeaT*1 protein at the molecular level such as the unfolding, the expansion of bondlengths, and the transform of the secondary structures, but the overlap between the high-temperature SAXS shapes with the room-temperature domain structures or with the predicted ones are still significant. At least, this overlap can give the clue to insight into the structural changes. The overlaps of the structural domains on the overall shape of *PeaT*1 homodimer are shown in Figure 6. The SAXS shapes are plotted with mesh envelopes and the "crystal" structures of the four domains are shown in "spacefill" mode of RASMOL. The two homologous molecules included respectively four structural domains are, respectively, represented with the warm and cool colors. The four domains in each molecule are distinguished by the color shade. From Figure 6, it can be seen that the two *PeaT*1 molecules were pushed away each other with temperature increase. Accompanying the position rotation and translation of the four domains, the two *PeaT*1 molecules had even a detached tendency at 85°C. It was these relative motions that causes the shape change and enlarges the D_{max} from 128Å to 139Å as the temperature increases from 25°C to 85°C.

Total eight domains were used to superimpose on the particle shape. The eight domains were classified into two homodimeric molecules. The two homodimeric molecules were restricted to be symmetrical along a P_2 axis. Each molecule includes *F*, *NAC*, *T*, and *UBA* four domains which are simply contacted together according to the amino acid sequence. The two Cα atoms connecting two adjacent domains were maintained to a constant Cα–Cα bondlength (~3.78 Å) which was obtained by averaging the nearest-near Cα–Cα distances over all Cα atoms in the four domains. Figure 8 shows the conformation change of *PeaT*1 single molecule with temperature in a ribbon mode. The corresponding sequence numbers of the *PeaT*1 protein molecule are also labeled in Figure 8. The description of the domain position changes is quite complicated. Here, six parameters ($x0$, $y0$, $z0$; α, β, γ) can be used to describe the position changes of each domain in a *PeaT*1 molecule. ($x0$, $y0$, $z0$) describe the coordinates of the rotating center of each domain, which is coordinated with the first Cα atom in domain-(1), or the last Cα atom in domain-(n − 1) as rotating the domain-(n). α describes the rotation angle of the domain along the *Z*-axis. β describes the rotation angle of the domain along the *C*-axis defined by the tie line between the domain centroid and the rotating center. γ describes the rotation angle of the domain along the *B*-axis which is perpendicular to the *Z*-axis and *C*-axis, and pass through the rotating center. The rotation angles (α, β, γ) and the coordinates ($x0$, $y0$, $z0$) of the four domains at the measurement temperatures are listed in Table II. The centroidal distance between the two molecules in a *PeaT*1 homodimer is calculated to be 13.4, 23.4, 27.2, 14.6, and 16.4 Å for the samples 251, 551, 851, 552, and 252, respectively. This centroidal distance has an increasing trend with the temperature rising. Evidently, the four structural domains (*F*, *NAC*, *T*, and *UBA*) all have a position change with temperature, but the position of *NAC* is relatively stable, and the position changes of *F*, *T*, and *UBA* are relatively larger. Generally

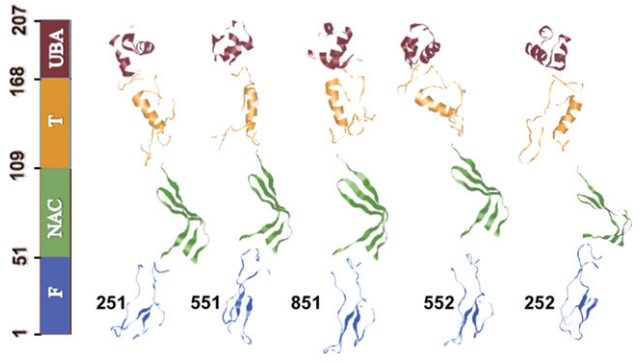

Figure 8

One molecule show: structural changes with temperature in one molecule of *PeaT*1 homodimer. Numerals 251, 551, 851, 552, and 252 mark, respectively, the protein being heated to 25, 55, and 85°C, then cooled to 55 and 25°C. The amino acid sequence numbers of the four structural domains (*F*, *NAC*, *T*, and *UBA*) are also shown in this Figure. Their predicted structures are distinguished by different colors. [Color figure can be viewed in the online issue, which is available at wileyonlinelibrary.com.]

Table II
Rotation Angles (α, β, γ) and Coordinates (*x*0, *y*0, *z*0) of the Rotating Center of Each Domain, Which is Coordinated With the first Cα Atom in Domain-(1), or the Last Cα Atom in Domain-(n-1) as Considering the Domain-(*n*). α is the Rotation Angle of Each Domain Along the *Z*-axis. β is the Rotation Angle of Each Domain Along the *C*-axis Defined by the Tie Line Between the Domain Centroid and the Rotating Center. γ is the Rotation Angle of Each Domain Along the *B*-axis Which is Perpendicular to the *Z*-axis and *C*-axis, and Pass Through the Rotating Center

Domains	Rotation angles or coordinates	Samples				
		251	551	851	552	252
F	α (degree)	67.0	96.6	0.0	39.2	0.0
	β (degree)	303.9	100.1	2.5	4.7	35.4
	γ (degree)	225.8	156.0	181.4	91.8	177.1
	*x*0 (Å)	6.268	5.641	6.506	−6.495	18.219
	*y*0 (Å)	−0.599	21.433	3.762	1.520	−0.465
	*z*0 (Å)	28.675	36.109	27.764	−29.555	31.990
NAC	α (degree)	65.5	47.6	0.0	108.2	37.3
	β (degree)	356.8	283.6	100.2	79.6	32.5
	γ (degree)	59.4	40.6	359.4	317.0	70.7
	*x*0 (Å)	11.248	10.581	16.412	−17.335	16.515
	*y*0 (Å)	−11.091	13.448	8.152	1.333	−11.097
	*z*0 (Å)	29.005	29.263	23.566	−25.374	27.624
T	α (degree)	83.7	0.4	29.1	26.7	0.0
	β (degree)	92.4	282.8	271.5	18.2	31.7
	γ (degree)	223.9	28.1	86.7	260.4	110.4
	*x*0 (Å)	−1.366	12.455	8.510	−3.668	11.146
	*y*0 (Å)	−13.573	11.794	−4.041	−7.567	11.229
	*z*0 (Å)	−18.097	−18.927	−21.343	24.786	−14.274
UBA	α (degree)	20.0	0.0	170.0	174.6	4.3
	β (degree)	90.4	343.0	322.7	16.0	22.0
	γ (degree)	93.3	164.2	226.2	235.9	107.1
	*x*0 (Å)	2.110	−0.794	18.130	7.424	0.737
	*y*0 (Å)	4.439	6.561	2.145	−3.327	−2.804
	*z*0 (Å)	−42.607	−39.815	−46.951	46.769	−40.536

speaking, the random coils in *PeaT*1 protein could not be really back to their initial state after a heating–cooling process. In fact, the four structural domains were all not exactly returned to their initial positions. Although the SRCD results demonstrated that the percentages of the secondary structures are recoverable, we believe that the secondary structures, especially the random coil structures, in *PeaT*1 homodimer can not completely recover their initial state. In the shape overlap, the four domains were supposed to have rigid structures, and only their relative positions were adjusted and optimized by using the simulated annealing algorithm. This is because of the shortage of the known structures of the domains at high-temperatures. Especially, the random coiled structure of domain *F* is difficult to be confirmed. According to the SRCD results, the percentage change of the secondary structures will lead to the structural changes of domains *F*, *NAC*, *T*, and *UBA*. The content decrease of α-helices and β-turns as well as the content increase of random coils demonstrated that partial α-helices (about 63%) and β-turns (about 32%) were transformed into random coils when the temperature was increasing. However, the percentage of β-strands was almost unchangeable. From Figure 8, it can be seen that most of α-helices exist in domain *UBA* and a few exist probably in domains *T*, while the β-strands are mainly existent in domains *NAC*, and partially existent in domains *F* and/or *T*. These imply that the atomic structures in domains *UBA* and *T* are easy to change, while the atomic structures in domain *NAC* tends to unchanged. The variability with temperature of *F*, *T*, and *UBA* structures should also be reflected in these changes of domain relative position and *PeaT*1 protein shape. Indeed, the positions of *T* and *UBA* domains have larger changes, which results in a shape change of *PeaT*1 from gooseneck vase-like, to jug-like, then to oval shape with temperature increase. Although we have to suppose that the domain structures are rigid in the overlap process between the SAXS shape and the domain configuration, the changes of domain position with temperature still reflect the relative motion of the four domains and the structural evolution of *PeaT*1 protein. Combining the SAXS and SRCD results, we think that α-helices in proteins are preferentially transformed into random coils compared with β-strands in a heating process. That is to say, on comparison with β-strands, α-helices in proteins are more mutable.

This SAXS study gives a low-resolution structure of *PeaT*1 protein and its structural evolution with temperature. For the thermotolerance of *PeaT*1 protein, we have a detailed discussion. We expect this study is helpful to understanding further the biological function of *PeaT*1 protein and its agricultural application as a pesticide.

CONCLUSIONS

SAXS techniques combined with SRCD results were used to investigate the low-resolution structure of *PeaT*1 protein in solution as well as the structural evolution with temperature. *PeaT*1 protein was identified to contain 207 amino acids, which are divided into four structural domains (*F*, *NAC*, *T*, and *UBA*). In the solution, *PeaT*1 protein presents a thermotolerant characteristic and forms a homodimeric structure, each molecule contains *F*, *NAC*, *T*, and *UBA* four structural domains. SRCD revealed that the secondary structures in *PeaT*1 protein are reversible with temperature change. SAXS demonstrated that the shape change of *PeaT*1 protein in solution is also approximately reversible with temperature change. During the heating process, *PeaT*1 protein experiences a gooseneck vase-like (25°C), to jug-like (55°C), then to oval (85°C) shape change. At the same time, the two molecules are pushed away each other. In the subsequent cooling process, the protein shape recovers again to the jug-like (55°C) and the gooseneck vase-like (25°C) shapes. Simultaneously, the two molecules were attracted to close up. During a heating–cooling cycle, all structural domains have a relative position rotation or translation. Domains *F*, *T* and *UBA* are more mutable than *NAC* during a heating–cooling cycle, which

will results in main shape changes. However, the two *NAC* domains hug together face to face, and their relatively stable structure play a crucial role of frame in the thermotolerance of *PeaT*1 protein. Through the reversible structural relaxation, *PeaT*1 protein presents a higher thermotolerance.

REFERENCES

1. Muller M. Alternaria infestation of corn silage and hay. Zentralbl Mikrobiol 1991;146:481–488.
2. Mao J, Liu Q, Yang X, Long C, Zhao M, Zeng H, Liu H, Yuan J, Qiu D. Purification and expression of a protein elicitor from *Alternaria tenuissima* and elicitor-mediated defense responses in tobacco. Ann Appl Biol 2010;156:411–420.
3. Finn RD, Tate J, Mistry J, Coggill PC, Sammut JS, Hotz HR, Ceric G, Forslund K, Eddy SR, Sonnhammer EL, Bateman A. The Pfam protein families database. Nucleic Acids Res 2008;36:D281–288.
4. Andersen KM, Semple CA, Hartmann-Petersen R. Characterisation of the nascent polypeptide-associated complex in fission yeast. Mol Biol Rep 2007;34:275–281.
5. Spreter T, Pech M, Beatrix B. The crystal structure of archaeal nascent polypeptide-associated complex (NAC) reveals a unique fold and the presence of a ubiquitin-associated domain. J Biol Chem 2005;280:15849–15854.
6. Liu Q, Li T, Yang X, Zeng H, Qiu DW. Research on the heat resistance of protein elicitor PeaT1 by synchrotron radiation circular dichroism. J Agric Biotech 2010;18:592–596. (In Chinese)
7. Li SJ, Hong XG, Shi YY, Li H, Wang CC. Annular arrangement and collaborative actions of four domains of protein-disulfide isomerase: a small angle X-ray scattering study in solution. J Biol Chem 2006;281:6581–6588.
8. Lamb J, Kwok L, Qiu X, Andresen K, Park HY, Pollack L. Reconstructing three-dimensional shape envelopes from time-resolved small-angle X-ray scattering data. J Appl Crystallogr 2008;41:1046–1052.
9. Chacón P, Morán F, Díaz JF, Pantos E, Andreu JM. Low-resolution structures of proteins in solution retrieved from X-ray scattering with a genetic algorithm. Biophys J 1998;74:2760–2775.
10. Matozo HC, Santos MA, de Oliveira Neto M, Bleicher L, Lima LM, Iuliano R, Fusco A, Polikarpov I. Low-resolution structure and fluorescence anisotropy analysis of protein tyrosine phosphatase eta catalytic domain. Biophys J 2007;92:4424–4432.
11. Dong SQ, Li LQ, Liu P, Dong YH, Chen XM. Investigation of the topological shape of bovine serum albumin in solution by small-angle x-ray scattering at Beijing synchrotron radiation facility. Chin Phys C 2008;17:4574–4579.
12. Huang YS, Jeng US, Shiu YJ, Lai YH, Sun YS. Charge interaction and temperature effects on the solution structure of lysozyme as revealed by small-angle x-ray scattering. J Appl Crystallogr 2007;40:s165–169.
13. Shiu YJ, Jeng US, Huang YS, Lai YH, Lu HF, Liang CT. Global and local structural changes of cytochrome c and lysozyme characterized by a multigroup unfolding process. Biophys J 2008;94:4828–4836.
14. Shilton B, Svergun DI, Volkov VV, Koch MH, Cusack S, Economou A. *Escherichia coli* SecA shape and dimensions. FEBS Lett 1998;436:277–282.
15. Shi YY, Hong XG, Wang CC. The C-terminal (331–376) sequence of Escherichia coli DnaJ is essential for dimerization and chaperone activity: a small angle X-ray scattering study in solution. Biol Chem 2005;280:22761–22768.
16. Zipper P, Durchschlag H. Ab initio reconstructions of the shape of cellobiose dehydrogenase and its domains in solution. Phys Script 2005;T118:228–232.
17. Ashish , Garg R, Anguita J, Krueger JK. Binding of full-length HIV-1 gp120 to CD4 induces structural reorientation around the gp120 core. Biophys J 2006;91:L69–L71.
18. Svergun DI, Volkov VV, Kozin MB, Stuhrmann HB. "New developments in direct shape determination from small-angle scattering. 2. Uniqueness." Acta Crystallogr Sect A 1996;52:419–426.
19. Svergun DI, Petoukhov MV, Koch MH. Determination of domain structure of proteins from X-ray solution scattering. Biophys J 2001;80:2946–2953.
20. Svergun DI. Advanced solution scattering data analysis methods and their applications. J Appl Crystallogr 2000;33:530–534.
21. Svergun DI. Restoring low resolution structure of biological macromolecules from solution scattering using simulated annealing. Biophys J 1999;76:2879–2886.
22. Bradford MM. "Rapid and sensitive method for the quantitation of microgram quantities of protein utilizing the principle of protein-dye binding." Anal Biochem 1976;72:248–254.
23. Gill SC, von Hippel PH. Calculation of protein extinction coefficients from amino acid sequence data Anal Biochem 1989;182:319–326.
24. Hammersley AP. ESRF website:http://www.esrf.eu/computing/scientific/FIT2D/. V12.012. 2004.
25. Konarev PV, Volkov VV, Sokolova AV, Koch MH, Svergun DI. PRIMUS: a Windows PC-based system for small-angle scattering data analysis. J Appl Crystallogr 2003;36:1277–1282.
26. Putnam CD, Hammel M, Hura GL, Tainer JA. X-ray solution scattering (SAXS) combined with crystallography and computation: defining accurate macromolecular structures, conformations and assemblies in solution. Q Rev Biophys 2007;40:191–285.
27. Glatter O, Kratky O. Small-Angle X-Ray Scattering. London: Academic Press; 1982. p25, p6.
28. Svergun DI. Mathematical methods in small-angle scattering data analysis. J Appl Crystallogr 1991;24:485–492.
29. Semenyuk AV, Svergun DI. GNOM—a program package for small-angle scattering data processing. J Appl Crystallogr 1991;24:537–540.
30. Svergun DI. Mathematical methods in small-angle scattering data analysis. J Appl Crystallogr 1992;25:495–503.
31. Beatrix B, Sakai H, Wiedmann M. The alpha and beta subunit of the nascent polypeptide-associated complex have distinct functions. J Biol Chem 2000;275:37838–37845.
32. Wiedmann B, Sakai H, Davis TA, Wiedmann M. A protein complex required for signal-sequence-specific sorting and translocation. Nature 1994;370:434–440.
33. Svergun DI, Koch MH. "Small-angle scattering studies of biological macromolecules in solution." Rep Prog Phys 2003;66: 1735–1782.
34. Svergun DI. Restoring low resolution structure of biological macromolecules from solution scattering using simulated annealing. Biophys J 1999;76:2879–2886.
35. Kozin MB, Svergun DI. Automated matching of high- and low-resolution structural models. J Appl Crystallogr 2001;34:33–41.
36. Volkov VV, Svergun DI. Uniqueness of ab initio shape determination in small- angle scattering. J Appl Crystallogr 2003;36:860–864.
37. Sayle RA, Milner-White EJ. RASMOL: biomolecular graphics for all. Trends Biochem Sci 1995;20:374–376.
38. Available at:http://cbsuapps.tc.cornell.edu/loopp.aspx, accessed on June 29, 2010.